

Article

Numerical Study of the Gas-Liquid Two-Phase Flow in a Self-Designed Mixer for a Ga-R113 MHD System

Peng Lu ^{1,*} , Xingwen Zheng ¹, Lulu Fang ¹, Hulin Huang ^{2,*}, Shu Xu ³ and Yezhen Yu ⁴

¹ Jiangsu Province Key Laboratory of Aerospace Power System, Key Laboratory of Thermal Environment and Thermal Structure for Aero Engines of Ministry of Industry and Information Technology, College of Energy and Power Engineering, Nanjing University of Aeronautics and Astronautics, Nanjing 210016, China; zwx545469962@gmail.com (X.Z.); 18662705220fdl@gmail.com (L.F.)

² College of Astronautics, Nanjing University of Aeronautics and Astronautics, Nanjing 210016, China

³ Department of Chemical Engineering, Purdue University, West Lafayette, IN 47907, USA; richard041123@gmail.com

⁴ School of Energy and Mechanical Engineering, Nanjing Normal University, Nanjing 210042, China; yuyezhen@njnu.edu.cn

* Correspondence: plu@nuaa.edu.cn (P.L.); hlhuang@nuaa.edu.cn (H.H.); Tel.: +86-25-8489-6183 (H.H.)

Received: 29 September 2017; Accepted: 15 October 2017; Published: 17 October 2017

Abstract: Liquid metal MHD (Magneto-Hydro-Dynamic) systems can be employed to produce electricity from a wide range of heat resources. In such a system, a low-boiling organic fluid and a high-temperature liquid metal fluid mix. The former evaporates, and carries the latter to flow through an MHD channel, where the electricity is generated. The mixing process and the gas-liquid flow characteristics will have a significant effect on the power generating efficiency. In the present work, trifluorotrichloroethane (R113) was chosen as the organic fluid, and gallium (Ga) as the liquid metal, respectively. Numerical study was subsequently carried out on the gas-liquid flow and heat transfer in a self-designed spherical mixer. The effects of the main factors, including the inlet velocities and inlet temperatures of Ga and R113, were separately determined, with suggested values or ranges discussed in detail.

Keywords: Magneto-Hydro-Dynamic (MHD); gas-liquid two-phase flow; numerical study; mixer

1. Introduction

At present, the ever-increasing energy cost, shortage of fossil fuel resources, and environmental pollution have aroused the development of high-efficiency energy conversion technologies [1]. MHD power-generation technology extends Faraday's law to conductive fluids [2], which can be classified into high-temperature plasma MHD systems and LMMHD (Liquid Metal MHD) systems, based on the sort of working medium.

In high-temperature plasma MHD systems, the working gas has to be ionized at a very high temperature, usually up to over 5000 K [3,4], so as to reach an appropriate electrical conductivity [5]. Although ionization seeds can be used to lower this temperature, it still exceeds 2000~2500 K [6,7]. In addition, there is another crucial technical problem to overcome—the slagging [8].

Compared to high-temperature plasma MHD systems, LMMHD systems have no such problems. There are typically two types of fluids in an LMMHD system: the thermodynamic fluid (low-boiling organic medium) and the power-generating fluid (conductive liquid metal). The thermal efficiency is theoretically close to the Carnot cycle in that the low-boiling organic medium is continuously heated by the high-temperature liquid metal [9]. More significantly, LMMHD systems can be utilized for a wide range of heat resources, including solar, geothermal, fossil fuels, nuclear, and chemical reactions, etc.

The schematic of a two-phase LMMHD system is shown in Figure 1. The liquid metal is first heated up in the heater. In the mixer, the two fluids mix and the low-boiling organic medium evaporates. Subsequently, the gas-liquid two-phase fluids flow through the MHD generator and electricity is created. Finally, the fluids are separated and pumped back to the mixer through the upper and lower loops, respectively.

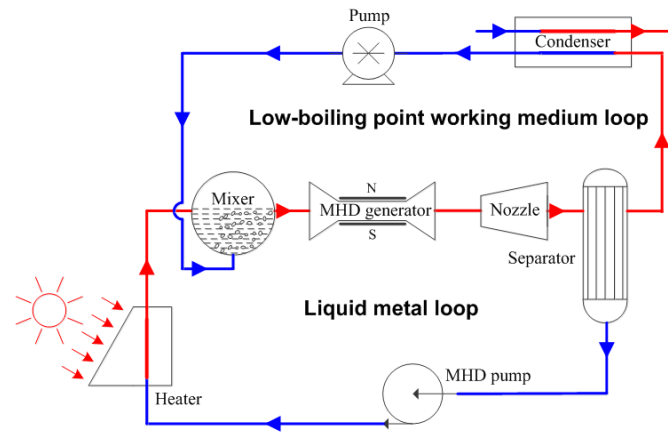


Figure 1. Schematic of a two-phase LMMHD system.

LMMHD systems are drawing increasing attention on various topics, including flow and heat transfer [10–12], magnetic effects [13,14], power-generating characteristics [15], and bubble behaviours [16], etc. For example, Kakarantzas et al. [12] investigated the MHD liquid metal flow and heat transfer in vertical annuli under a horizontal magnetic field by direct numerical simulations. They found that the fluid motion increases with the aspect ratio and annular gap, and the highest spatially averaged heat transfer rates are obtained for aspect ratios equal to one. Bakalis and Hatzikonstantinou [14] studied the MHD flow of a liquid metal in a curved annular channel, so as to examine the effect of curvature and the magnetic field on the velocity distribution. Schwarz and Froehlich [16] numerically simulated the upward motion of a single bubble in liquid metal exposed to an external magnetic field. The results showed that for large bubbles, the rise velocity increases first and then decreases; on the other hand, for small bubbles, the rise velocity decreases when strengthening the magnetic field.

However, there are rather few studies focusing on the mixing process and two-phase flow characteristics inside the mixer which can significantly affect the follow-up power-generation process. In our previous research, with tin and trifluorotrchloroethane (R113) chosen as the liquid metal and low-boiling working medium, respectively, a preliminary two dimensional numerical study was carried out on the two-phase flow characteristics [2]. Further research on the effects of the physical properties of liquid metal indicates that, compared to tin, Gallium (Ga) has a more beneficial influence on the flow and heat transfer process due to its higher heat capacity and conductivity [17]. Therefore, in the present paper, we will advance the research on a self-designed spherical mixer for two-phase LMMHD systems, with Ga and R113 as the working media. Their physical properties are presented in Tables 1 and 2. A three-dimensional numerical study will be carried out, aiming to determine the effects of the main impacting factors on the gas-liquid two-phase flow characteristics.

Table 1. Physical properties of Ga.

Physical Properties	Liquid Gallium
Molar mass ($\text{g}\cdot\text{mol}^{-1}$)	69.723
Density ($\text{kg}\cdot\text{m}^{-3}$)	5904
Melting point (K)	303
Heat capacity ($\text{J}\cdot\text{kg}^{-1}\cdot\text{K}^{-1}$)	383.52
Heat conductivity ($\text{W}\cdot\text{m}^{-1}\cdot\text{K}^{-1}$)	58
Viscosity ($\text{kg}\cdot\text{m}^{-1}\cdot\text{s}^{-1}$)	1.94×10^{-3}

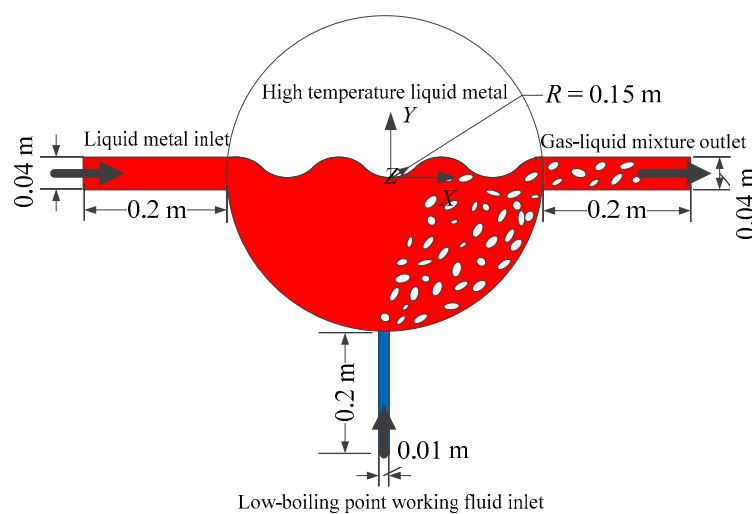
Table 2. Physical properties of R113 and R113 gas (R113 g).

Physical Properties	R113	R113 g
Molar mass ($\text{g}\cdot\text{mol}^{-1}$)	187.376	187.376
Density ($\text{kg}\cdot\text{m}^{-3}$)	1565	7.38
Boiling point (K)	321	—
Latent heat of vaporization ($\text{kJ}\cdot\text{kg}^{-1}$)	146.7	—
Heat capacity ($\text{J}\cdot\text{kg}^{-1}\cdot\text{K}^{-1}$)	912	673
Heat conductivity ($\text{W}\cdot\text{m}^{-1}\cdot\text{K}^{-1}$)	0.0657	0.0778
Viscosity ($\text{kg}\cdot\text{m}^{-1}\cdot\text{s}^{-1}$)	4.97×10^{-4}	1.08×10^{-5}
Standard-state enthalpy ($\text{J}\cdot\text{kmol}^{-1}$)	-8×10^8	-6.95×10^8

2. Modelling

2.1. Model Set-Up

A self-designed mixer modeled by Unigraphics (UG) is shown in Figure 2. High-temperature liquid Ga is initially stored inside this adiabatic spherical mixer. R113 and liquid Ga enter the mixer from the bottom and left inlets, respectively. Once R113 makes contact with liquid Ga, it is heated up and evaporates into gas. The continuous expansion of R113 gas increases the inner pressure, and pushes the two-phase fluids out of the mixer from the right outlet. This mixer features a simple structure, and provides an appropriate route and space for mixing, flow, and heat transfer, especially for such gas-liquid two-phase media. In this way, the flow velocity is accelerated to a much higher value at the outlet, which is of great benefit to the electrical power generating in the follow-up MHD generator.

**Figure 2.** The self-designed mixer model built by UG.

2.2. Numerical Model

2.2.1. Governing Equations

The multiphase models in FLUENT can be classified into the VOF (Volume of Fluid) model, Mixture model, and Eulerian model. Among them, the Mixture model is relatively suitable for simulating the mixing process of R113 and Ga, in combination with a standard $k-\varepsilon$ two-equation turbulent model. In addition, the SIMPLE scheme is applied to resolve the pressure-velocity coupling equation, and the second-order upwind difference scheme is used for discretization, with the convergence precision of 10^{-6} to obtain a satisfactory accuracy. The governing equations [18] are as follows.

(1) Continuity Equation

$$\frac{\partial}{\partial t}(\rho_m) + \nabla \cdot (\rho_m \vec{v}_m) = 0 \quad (1)$$

(2) Momentum Equation

$$\frac{\partial}{\partial t}(\rho_m \vec{v}_m) + \nabla \cdot (\rho_m \vec{v}_m \vec{v}_m) = -\nabla p + \nabla \cdot \left[\mu_m (\nabla \vec{v}_m + \nabla \vec{v}_m^T) \right] + \rho_m \vec{g} + \vec{F} + \nabla \cdot \left(\sum_{k=1}^n \alpha_k \rho_k \vec{v}_{dr,k} \vec{v}_{dr,k} \right); \quad (2)$$

where \vec{v}_m is the mass-averaged velocity $\frac{\sum_{k=1}^n \alpha_k \rho_k \vec{v}_k}{\rho_m}$, ρ_m is the mixture density $\sum_{k=1}^n \alpha_k \rho_k$, n is the number of phases, \vec{F} is the body force, α_k is the volume fraction of phase k , μ_m is the viscosity of the mixture $\sum_{k=1}^n \alpha_k \mu_k$, and $\vec{v}_{dr,k}$ is the drift velocity of phase k .

(3) Energy Equation

$$\frac{\partial}{\partial t} \sum_{k=1}^n (\alpha_k \rho_k E_k) + \nabla \cdot \sum_{k=1}^n \left[\alpha_k \vec{v}_k (\rho_k E_k + p) \right] = \nabla \cdot (k_{\text{eff}} \nabla T) + S'; \quad (3)$$

E_k is the energy of phase k ; S' is the volumetric heat sources; and k_{eff} is the effective thermal conductivity $\sum_{k=1}^n \alpha_k (k_k + k_t)$, where k_k is the thermal conductivity of phase k and k_t is the turbulent thermal conductivity.

(4) Volume fraction equation of the second phase

$$\frac{\partial}{\partial t}(\alpha_k \rho_k) + \nabla \cdot (\alpha_k \rho_k \vec{v}_k) = -\nabla \cdot (\alpha_k \rho_k \vec{v}_{dr,k}). \quad (4)$$

A simple and accurate model proposed by Lee [19] and widely acknowledged is employed in the present paper to calculate the evaporation process of R113, with the relevant source terms expressed as follows.

R113 source term:

$$S_M = -r \alpha_R \rho_R \left(\frac{T - T_b}{T_b} \right); \quad (5)$$

R113 (gas) source term:

$$S_M = r \alpha_R \rho_R \left(\frac{T - T_b}{T_b} \right); \quad (6)$$

Energy source term:

$$S_E = -r \alpha_R \rho_R \left(\frac{T - T_b}{T_b} \right) \Delta H. \quad (7)$$

where S_M and S_E are the mass and energy source terms, respectively; α_R and ρ_R are the volume fraction and density of R113; T and T_b are the mixture temperature and boiling point of R113; ΔH is the latent heat; and r is the phase change factor.

2.2.2. Boundary Conditions

The velocity-inlet and pressure-outlet boundary conditions are applied to the computational domain, where the outlet pressure is set as the standard atmosphere. The boundary conditions for the pipe wall are impermeable, non-slip, and adiabatic, with an inner roughness at 5×10^{-5} m. Gravity acceleration is taken into consideration, whereas the radiant heat exchange between the working media is ignored.

2.2.3. Independence Verification

The 3D computational domain with meshes is depicted in Figure 3. The mesh number has a great influence on the simulation accuracy. Generally, increasing the mesh number will, on the one hand, obtain more accurate simulation results; on the other hand, it will result in a much longer computing time. In order to balance the simulation accuracy and computing time, it is necessary to perform the verification of grid independence.

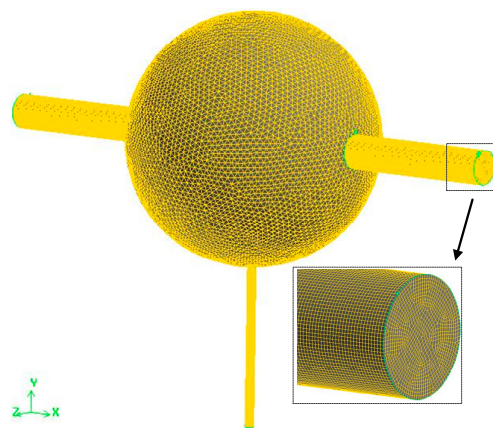


Figure 3. The 3D computational domain with meshes.

The mesh number is set as 2.1×10^5 , 3.7×10^5 , 6.0×10^5 , 8.9×10^5 , and 12.1×10^5 , respectively, and the corresponding outlet velocity (v_{lmo}) and volume fraction of liquid Ga (VF_o) are plotted in Figure 4. It can be seen that the values fluctuate after the mesh number exceeds 6.0×10^5 , which can be consequently recognized as the appropriate mesh number.

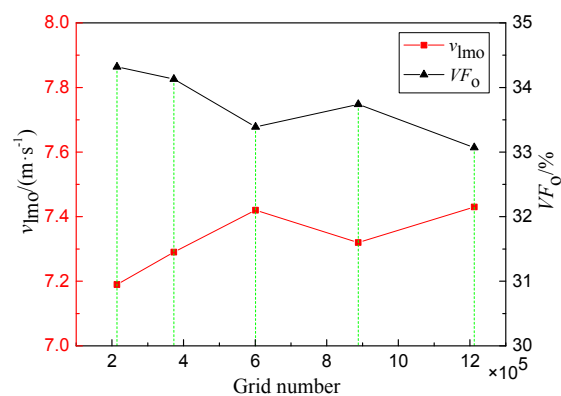


Figure 4. Independent verification of grid number.

The numerical method in this paper is testified by simulating a gas-liquid flow process in the literature [20], as shown in Figure 5. The figure describes the axial pressure distribution at different Reynolds numbers, and the simulated results acquired by the present method are in good agreement with the experiments, with the maximum error of less than 10%.

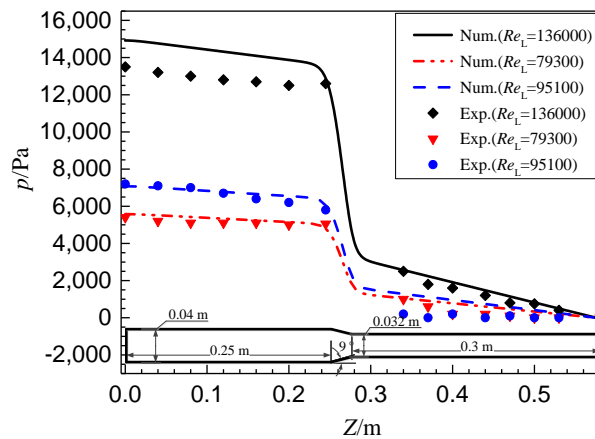


Figure 5. Comparison of the simulated results with the experimental data in the literature.

3. Results and Discussion

3.1. Effects of v_{lmi}

The volume fraction distribution of liquid Ga (VF) and the flow field across the longitudinal section ($Z = 0$) under different inlet velocities of liquid Ga (v_{lmi}) are depicted in Figure 6. As v_{lmi} increases, the falling position of liquid Ga gradually rises, and the evaporation area (or mixing area) enclosed by the high-temperature Ga enlarges, which is beneficial to R113 evaporation.

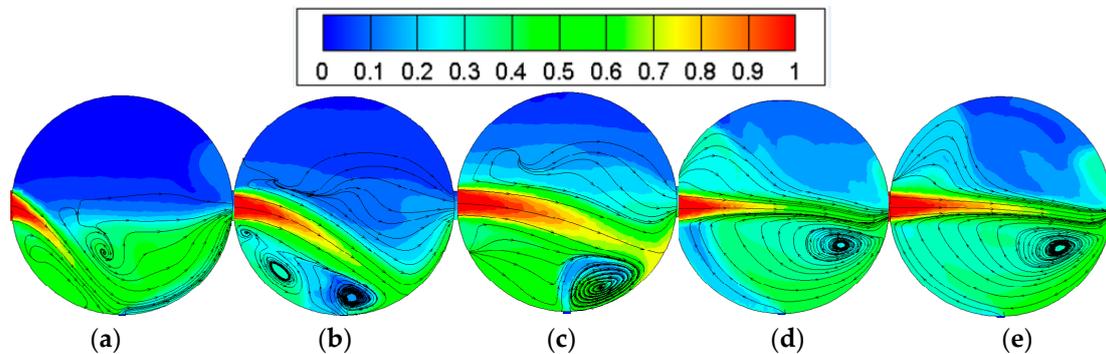


Figure 6. VF distribution and flow field across the longitudinal section ($Z = 0$) under different v_{lmi} : (a) $v_{lmi} = 0.6 \text{ m}\cdot\text{s}^{-1}$; (b) $v_{lmi} = 1.2 \text{ m}\cdot\text{s}^{-1}$; (c) $v_{lmi} = 1.8 \text{ m}\cdot\text{s}^{-1}$; (d) $v_{lmi} = 2.4 \text{ m}\cdot\text{s}^{-1}$; (e) $v_{lmi} = 3.0 \text{ m}\cdot\text{s}^{-1}$.

The controlling variables method is applied in the present paper. Keeping the inlet temperature of Ga (T_{lmi}), inlet velocity of R113 (v_{Ri}), and inlet temperature of R113 (T_{Ri}) constant at 573 K, $0.6 \text{ m}\cdot\text{s}^{-1}$, and 310 K, respectively, the inlet velocity of liquid Ga (v_{lmi}) varies from $0.6 \text{ m}\cdot\text{s}^{-1}$ to $3.0 \text{ m}\cdot\text{s}^{-1}$. It can be noticed from Figure 7 that as v_{lmi} increases, all of the outcomes rise, with the outlet velocity of Ga (v_{lmo}) increasing from $3.46 \text{ m}\cdot\text{s}^{-1}$ to $7.81 \text{ m}\cdot\text{s}^{-1}$, outlet volume fraction of Ga (VF_o) from 18.78% to 39.63%, and evaporation rate of R113 (ER) from 35.42% to 64.14%, respectively. It is understandable that more liquid Ga is provided due to the increasing inlet velocity. In addition, the evaporation area increases, as shown in Figure 6. They both facilitate the evaporating process and improve the

carrying ability of R113. As a result, v_{lmo} increases. Since more liquid Ga is supplied and conveyed, VF_o increases accordingly.

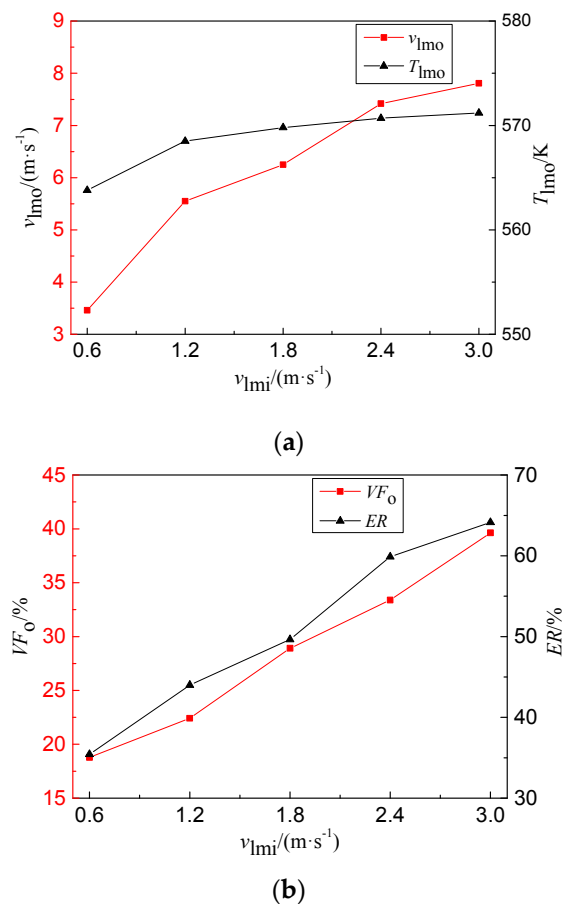


Figure 7. Impacts of v_{lmi} on the gas-liquid two-phase flow characteristics: (a) Impacts of v_{lmi} on the v_{lmo} and T_{lmo} ; (b) Impacts of v_{lmi} on the VF_o and ER .

Although in general, increasing v_{lmi} has a positive effect on the outlet flow characteristics, it should be pointed out that there should be a limit on it. Figure 7a shows that the outlet temperature of liquid Ga (T_{lmo}) is very close to its inlet temperature (573 K) when the velocity exceeds $2.4 m \cdot s^{-1}$, suggesting that the isothermal expansion of the two-phase mixture is realized and the optimal thermodynamic efficiency is achieved. A further increase of v_{lmi} will not obviously improve the evaporation area, as shown in Figure 6d,e. Conversely, it will consume more pump power and reduce the overall efficiency of the system. Taking the above factors into consideration, the suggested range for v_{lmi} is between $1.8 m \cdot s^{-1}$ and $2.4 m \cdot s^{-1}$.

3.2. Effects of T_{lmi}

Keeping the inlet velocity of liquid Ga (v_{lmi}), inlet velocity of R113 (v_{Ri}), and inlet temperature of R113 (T_{Ri}) constant at $2.4 m \cdot s^{-1}$, $0.6 m \cdot s^{-1}$, and 310 K, respectively, the variations of inlet temperature of liquid Ga (T_{lmi}) are presented in Figure 8. This figure shows that with T_{lmi} increasing, the outlet velocity of Ga (v_{lmo}) rises from $6.48 m \cdot s^{-1}$ to $8.59 m \cdot s^{-1}$, and the evaporation rate of R113 (ER) rises from 48.73% to 80.20%; whereas the outlet volume fraction of Ga (VF_o) declines from 38.33% to 29.10%. The rising T_{lmi} is beneficial to R113 evaporation; thus, the carrying-ability of R113 gas is promoted and the outlet velocity of Ga (v_{lmo}) rises. Nevertheless, the increasing volumetric proportion of R113 gas

will adversely reduce VF_o and the electrical conductivity of the fluids. The reason for keeping VF_o above a certain value will be subsequently discussed in further detail.

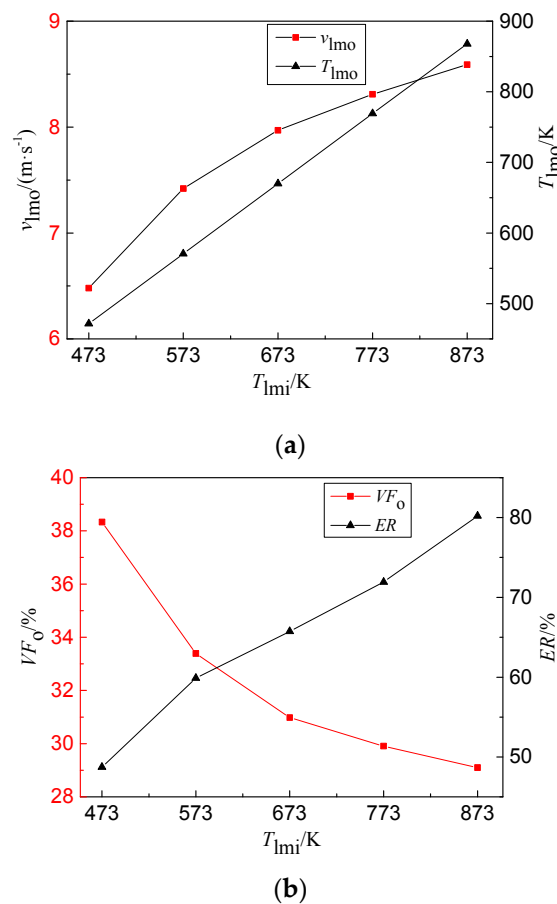


Figure 8. Impacts of T_{lmi} on the gas-liquid two-phase flow characteristics: (a) Impacts of T_{lmi} on the v_{lmo} and T_{lmo} ; (b) Impacts of T_{lmi} on the VF_o and ER .

3.3. Effects of v_{Ri}

Keeping the inlet velocity of liquid Ga (v_{lmi}), inlet temperature of liquid Ga (T_{lmi}), and inlet temperature of R113 (T_{Ri}) constant at $2.4 \text{ m}\cdot\text{s}^{-1}$, 573 K , and 310 K , respectively, the inlet velocity of R113 (v_{Ri}) ranges from $0.2 \text{ m}\cdot\text{s}^{-1}$ to $1.0 \text{ m}\cdot\text{s}^{-1}$. A higher v_{Ri} results in a higher R113 supply. As the thermodynamic fluid, its carrying-ability is enhanced. As a result, a higher outlet velocity of Ga (v_{lmo}) is obtained (Figure 9a) from $4.44 \text{ m}\cdot\text{s}^{-1}$ to $9.43 \text{ m}\cdot\text{s}^{-1}$. On the contrary, the outlet volume fraction of Ga (VF_o) declines from 55.61% to 26.81% due to the higher volumetric percentage of R113 gas. Because of the increased average velocity, the heat-transfer time length between the two fluids is reduced; thus, the evaporation rate of R113 (ER) decreases from 77.85% to 51.65% (Figure 9b). Still, it should be pointed out that VF_o should be controlled and this will be discussed in the next section.

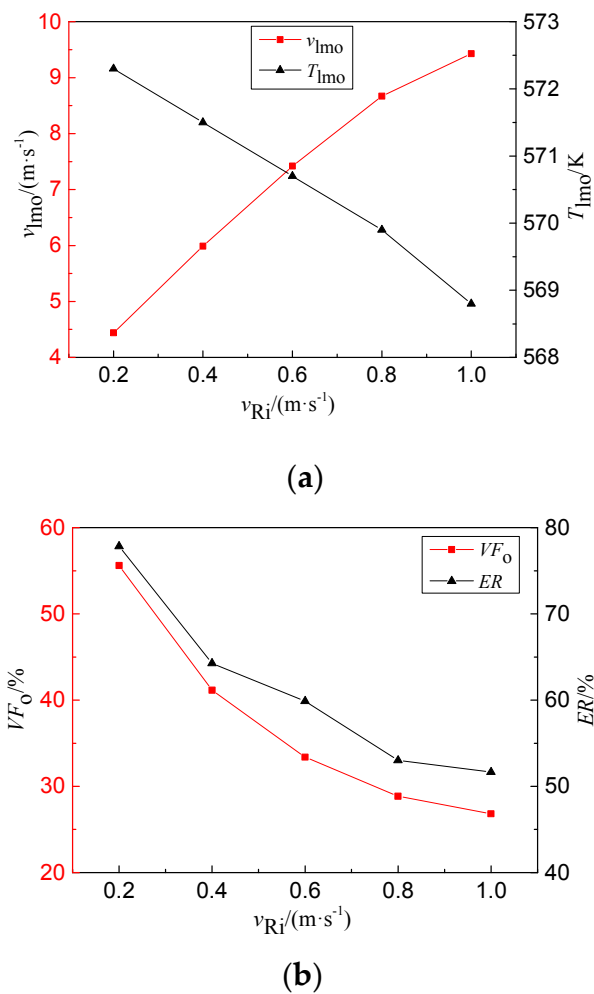


Figure 9. Impacts of v_{Ri} on the gas-liquid two-phase flow characteristics: (a) Impacts of v_{Ri} on the v_{lmo} and T_{lmo} ; (b) Impacts of v_{Ri} on the VF_o and ER .

3.4. Effects of T_{Ri}

Keeping the inlet velocity of liquid Ga (v_{lmi}), inlet temperature of liquid Ga (T_{lmi}), and inlet velocity of R113 (v_{Ri}) constant at $2.4 \text{ m}\cdot\text{s}^{-1}$, 573 K , and $0.6 \text{ m}\cdot\text{s}^{-1}$, respectively, the variations of inlet temperature of R113 (T_{Ri}) are presented in Figure 10. The temperature difference between the two fluids is reduced with T_{Ri} , which raises ER , and lowers VF_o slightly from 34.99% to 33.39% accordingly. Besides, since more R113 carrying gas is generated, the outlet velocity of Ga (v_{lmo}) rises from $7.17 \text{ m}\cdot\text{s}^{-1}$ to $7.42 \text{ m}\cdot\text{s}^{-1}$. Note that a very low VF_o may result in the R113 gas films covering the pipe walls in the follow-up MHD power-generating channel. In this situation, the annular flow pattern may be formed and leads to a loose contact between Ga and the electrodes. It is advised by Wallis [21] that VF_o be higher than 20% so as to avoid the above problem.

Specifically, Figure 11 provides more detailed distributions for three different volume fractions of Ga along $Y = 0$ at the outlet cross section. Note that at $VF_o = 50\%$ and $VF_o = 40\%$, the volume fraction of liquid Ga (VF) in the vicinity of the pipe wall is much higher than those at other locations, which is beneficial to power generation. However, with VF_o decreasing to 30% , the differences of VF among different locations are reduced, with the VF adjacent to the pipe wall decreasing dramatically from 67% to 37% . This indicates that the proportion of continuous R113 gas increases, which will have a detrimental impact on the power generating process by detaching the liquid metal from the electrodes.

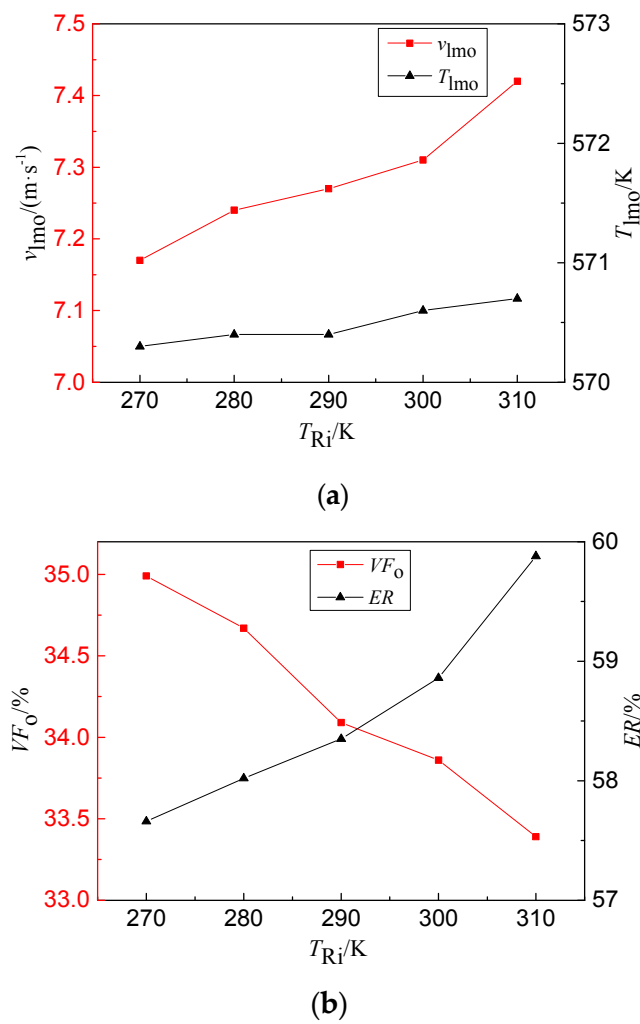


Figure 10. Impacts of T_{Ri} on the gas-liquid two-phase flow characteristics: (a) Impacts of T_{Ri} on the v_{lmo} and T_{lmo} ; (b) Impacts of T_{Ri} on the VF_o and ER .

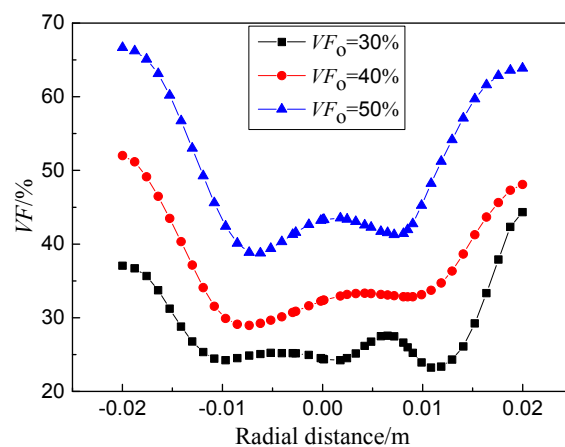


Figure 11. VF distributions along $Y = 0$ at the outlet cross section.

4. Conclusions

Liquid metal MHD systems can be utilized to produce electricity from varieties of heat resources. The mixing process and the gas-liquid flow characteristics will have a significant impact on the

power-generating efficiency. In the present work, a three-dimensional numerical study is conducted on the above process in a self-designed spherical mixer, with liquid metal gallium (Ga) selected as the working medium. The impacts of the main parameters are determined, respectively, with the conclusions as follows:

- (1) The evaporation area enlarges with the inlet velocity of liquid Ga (v_{limi}), which is beneficial to R113 evaporation.
- (2) Generally, increasing v_{limi} plays a positive role in the gas-liquid flow characteristics, because v_{limo} , VF_o and ER increase with v_{limi} . However, an excessively higher v_{limi} will result in an overload on the pump power, and consequently reduce the whole efficiency. The suggested range for v_{limi} is $1.8 \text{ m}\cdot\text{s}^{-1}$ to $2.4 \text{ m}\cdot\text{s}^{-1}$.
- (3) The inlet temperatures of liquid Ga (T_{limi}) and R113 (T_{Ri}) have similar impacts on the gas-liquid mixing and flow characteristics. With T_{limi} or T_{Ri} increasing, v_{limo} , T_{limo} , and ER rise, while VF_o declines. As the thermodynamic fluid, a higher inlet velocity of R113 (v_{Ri}) will, on one hand, obtain a higher v_{limo} ; on the other hand, it will reduce T_{limo} , ER, and VF_o .
- (4) It is suggested that VF_o be kept above a certain value. Otherwise an undesirable annular flow pattern may be formed, which has a detrimental impact on the power-generating process by detaching the liquid metal from the electrodes.
- (5) It is advised that future research work be centered on experimental investigations, microscopic bubble motions, economic performance, and commercialized operations in this field.

Acknowledgments: This work is supported by the “National Natural Science Foundation of China” (No. 11675077; 51506087); “Fundamental Research Funds” (No. JCKY2013203B003); “China Postdoctoral Science Foundation” (No. 2015M571747); “China Scholarship Council” (No. 201606835064); “the Fundamental Research Funds for the Central Universities” (No. NJ20160041); and the “Foundation of Graduate Innovation Center in Nanjing University of Aeronautics and Astronautics (NUAA)” (No. kfj20160210).

Author Contributions: Peng Lu took direct charge of this research. Hulin Huang provided ideas and instructions. Xingwen Zheng, Lulu Fang, Shu Xu, and Yezhen Yu participated in this research.

Conflicts of Interest: There are no conflicts of interest to declare.

Nomenclature

Symbols

E	energy	$\text{J}\cdot\text{kg}^{-1}$
ER	evaporation rate	%
\vec{F}	body force	N
\vec{g}	gravitational acceleration	$\text{m}\cdot\text{s}^{-2}$
k	thermal conductivity	$\text{W}\cdot\text{m}^{-1}\cdot\text{K}^{-1}$
n	number of phases	
p	pressure	Pa
R	radius	m
Re	Reynolds number	
r	the factor of phase change	s^{-1}
S	source term	$\text{kg}\cdot\text{m}^{-3}\cdot\text{s}^{-1}$ or $\text{kJ}\cdot\text{m}^{-3}\cdot\text{s}^{-1}$
S'	volumetric heat sources	$\text{W}\cdot\text{m}^{-3}$
t	time	s
T	temperature	K
v	velocity	$\text{m}\cdot\text{s}^{-1}$
\vec{v}	mass-average velocity	$\text{m}\cdot\text{s}^{-1}$
VF	volume fraction of liquid metal	%
X	axis X	m
Y	axis Y	m
Z	axis Z	m

Greek symbols

α	volume fraction	%
ΔH	latent heat	$\text{kJ}\cdot\text{kg}^{-1}$
ρ	density	$\text{kg}\cdot\text{m}^{-3}$
μ	viscosity	$\text{kg}\cdot\text{m}^{-1}\cdot\text{s}^{-1}$

Subscripts

b	boiling point
dr	drift
E	energy
eff	effective
i	inlet
k	phase k
l	liquid
lm	liquid metal
M	mass
m	mixture
o	outlet
R	R113
t	turbulence model

References

1. Koltsaklis, N.E.; Kopanos, G.M.; Georgiadis, M.C. Design and operational planning of energy networks based on combined heat and power units. *Ind. Eng. Chem. Res.* **2014**, *53*, 16905–16923. [[CrossRef](#)]
2. Lu, P.; Zheng, X.Y.; Yang, P.J.; Fang, L.L.; Huang, H.L. Numerical investigation into the vapor-liquid flow in the mixer of a liquid metal magneto-hydro-dynamic system. *RSC Adv.* **2017**, *7*, 35765–35770. [[CrossRef](#)]
3. Sakai, T.; Matsumoto, M.; Murakami, T.; Okuno, Y. Numerical simulation of power generation characteristics of a disk MHD generator with high-temperature inert gas plasma. *Electr. Eng. Jpn.* **2012**, *179*, 23–30. [[CrossRef](#)]
4. Tanaka, M.; Aoki, Y.; Zhao, L.; Okuno, Y. Experiments on high-temperature xenon plasma magnetohydrodynamic power generation. *IEEE Trans. Plasma Sci.* **2016**, *44*, 1241–1246. [[CrossRef](#)]
5. Komatsu, F.; Tanaka, M.; Murakami, T.; Okuno, Y. Experiments on high-temperature inert gas plasma MHD electrical power generation with hall and diagonal connections. *Electr. Eng. Jpn.* **2015**, *193*, 17–23. [[CrossRef](#)]
6. Li, Y.W.; Zhang, B.L.; Gao, L.; Duan, C.D.; Zhang, L.; Wang, Y.T.; He, G.Q. Research on generation and control of high temperature gas in MHD power generation. *J. Propuls. Technol.* **2017**, *38*, 1419–1426.
7. Tanaka, M.; Murakami, T.; Okuno, Y. Plasma characteristics and performance of magnetohydrodynamic generator with high-temperature inert gas plasma. *IEEE Trans. Plasma Sci.* **2014**, *42*, 4020–4025. [[CrossRef](#)]
8. Kayukawa, N. Open-cycle magnetohydrodynamic electrical power generation: A review and future perspectives. *Prog. Energy Combust. Sci.* **2004**, *30*, 33–60. [[CrossRef](#)]
9. Wu, Q.; Schubring, D.L.; Sienicki, J.J. Feasibility analysis of two-phase MHD energy conversion for liquid metal cooled reactors. *Nucl. Eng. Des.* **2007**, *237*, 2114–2119. [[CrossRef](#)]
10. Prinz, S.; Bandaru, V.; Kolesnikov, Y.; Krasnov, D.; Boeck, T. Numerical simulations of magnetohydrodynamic flows driven by a moving permanent magnet. *Phys. Rev. Fluids* **2016**, *1*. [[CrossRef](#)]
11. Sivakumar, R.; Vimala, S.; Sekhar, T.V.S. Influence of induced magnetic field on thermal MHD flow. *Numer. Heat Transf. A* **2015**, *68*, 797–811. [[CrossRef](#)]
12. Kakarantzas, S.C.; Benos, L.T.; Sarris, I.E.; Knaepen, B.; Grecos, A.P.; Vlachos, N.S. MHD liquid metal flow and heat transfer between vertical coaxial cylinders under horizontal magnetic field. *Int. J. Heat Fluid Flow* **2017**, *65*, 342–351. [[CrossRef](#)]
13. Rizzo-Sierra, J.A.; Lopez-Hernandez, O.I. Numerical study on the magnetohydrodynamics of an oscillatory flow under inductionless and core-side-layer approximations. *Rev. Mex. Fis.* **2016**, *62*, 369–380.
14. Bakalis, P.A.; Hatzikonstantinou, P.M. Effect of curvature and magnetic field on MHD flow of a liquid metal in a curved annular duct. *Int. J. Numer. Methods Heat Fluid Flow* **2015**, *25*, 1818–1833. [[CrossRef](#)]

15. Takahashi, R.; Matsuo, M.; Ono, M.; Harii, K.; Chudo, H.; Okayasu, S.; Ieda, J.; Takahashi, S.; Maekawa, S.; Saitoh, E. Spin hydrodynamic generation. *Nat. Phys.* **2016**, *12*, 52–56. [[CrossRef](#)]
16. Schwarz, S.; Froehlich, J. Numerical study of single bubble motion in liquid metal exposed to a longitudinal magnetic field. *Int. J. Multiph. Flow* **2014**, *62*, 134–151. [[CrossRef](#)]
17. Li, W.; Lu, P.; Zheng, X.W.; Huang, H.L. Numerical simulation of working fluid effects on two-phase flow in Immhd power generation system. *J. Jiangsu Univ. (Nat. Sci. Ed.)* **2017**, *38*, 434–439.
18. Fluent Inc. *Fluent User's Guild*; Fluent Inc.: Lebanon, NH, USA, 2006.
19. Lee, W.H. *A Pressure Iteration Scheme for Two-Phase Flow Modeling*; Hemisphere: Washington, DC, USA, 1980.
20. Ahmadpour, A.; Noori Rahim Abadi, S.M.A.; Kouhikamali, R. Numerical simulation of two-phase gas—Liquid flow through gradual expansions/contractions. *Int. J. Multiph. Flow* **2016**, *79*, 31–49. [[CrossRef](#)]
21. Wallis, G.B. *One-Dimensional Two-Phase Flow*; McGraw-Hill: New York, NY, USA, 1969.



© 2017 by the authors. Licensee MDPI, Basel, Switzerland. This article is an open access article distributed under the terms and conditions of the Creative Commons Attribution (CC BY) license (<http://creativecommons.org/licenses/by/4.0/>).